View Article Online
View Journal

Dalton Transactions

An international journal of inorganic chemistry

Accepted Manuscript

This article can be cited before page numbers have been issued, to do this please use: A. Volpe, M. Natali, C. Graiff, A. Sartorel, C. Tubaro and M. Bonchio, *Dalton Trans.*, 2020, DOI: 10.1039/C9DT04841C.

This is an Accepted Manuscript, which has been through the Royal Society of Chemistry peer review process and has been accepted for publication.

Accepted Manuscripts are published online shortly after acceptance, before technical editing, formatting and proof reading. Using this free service, authors can make their results available to the community, in citable form, before we publish the edited article. We will replace this Accepted Manuscript with the edited and formatted Advance Article as soon as it is available.

You can find more information about Accepted Manuscripts in the Information for Authors.

Please note that technical editing may introduce minor changes to the text and/or graphics, which may alter content. The journal's standard Terms & Conditions and the Ethical guidelines still apply. In no event shall the Royal Society of Chemistry be held responsible for any errors or omissions in this Accepted Manuscript or any consequences arising from the use of any information it contains.

ROYAL SOCIETY OF CHEMISTRY

rsc.li/dalton

View Article Online
DOI: 10.1039/C9DT04841C

ARTICLE

Novel Iridium complexes with N-heterocyclic dicarbene ligands in light-driven water oxidation catalysis: photon management, ligand effect and catalyst evolution

Received 00th January 20xx,
Accepted 00th January 20xx

DOI: 10.1039/x0xx00000x

Andrea Volpe,[a] Mirco Natali,*[b] Claudia Graiff,[c] Andrea Sartorel,*[a] Cristina Tubaro*[a] and Marcella Bonchio[a]

Iridium complexes [IrClCp*diNHC]PF_6, with N-heterocyclic dicarbene (diNHC) and pentamethylcyclopentadienyl (Cp*) ligands, have been investigated in light driven water oxidation catalysis within the $Ru(bpy)_3^{2+}/S_2O_8^{2-}$ cycle (bpy = 2,2'-bipyridine). In particular, the effect of different diNHC ligands was evaluated by employing the complex **1a** (diNHC = 1,1'-dimethyl-3,3'-ethylenediimidazol-2,2'-diylidene) and the novel and structurally characterised **2** (diNHC = 3,3'-ethylene-5,5'-dibromodiimidazol-2,2'-diylidene) and **3** (diNHC = 1,1'-dimethyl-dibenzimidazol-2,2'-diylidene). The presented results include: (i) a photon management analysis of the **1a**/$Ru(bpy)_3^{2+}/S_2O_8^{2-}$ system, revealing two regimes of O_2 evolution rate, being dependent on the light intensity at low photon flux, where the system reaches an overall quantum yield up to 0.17±0.1 (quantum efficiency 34±2%), while being independent of light intensity at high photon flux thus indicating a change of limiting step; (ii) a trend of O_2 evolution activity that follows the order **1a** > **2** > **3** both under low and high photon flux conditions, with the reactivity that is favoured by the electron donating nature of the diNHC ligand, quantified on the basis of the carbene carbon chemical shift; (iii) an analogous trend also in the bimolecular rate constants of electron transfer k_{ET} from the iridium species to photogenerated $Ru(bpy)_3^{3+}$, with k_{ET} values in the range $4.2 \div 6.1 \times 10^4$ $M^{-1}s^{-1}$, thus implying a significant reorganisation energy to the Iridium sphere; (iv) the evolution of **1a**, as the most active Ir species in the series, to mononuclear iridium species with lower molecular weight and originating from oxidative transformation of the organic ligand scaffold, as proven by converging UV-Vis, MALDI-MS and ^{1}H-NMR evidences. These results can be used for the further design and engineering of novel catalysts.

Introduction

Iridium complexes have retained a great interest in the field of water oxidation catalysis,[1–6,7] due to their high activity in terms of turnover number (TON), turnover frequency (TOF), low electrochemical overpotential (η), and high quantum yield in the case of light-driven cycles,[8] mostly exploiting the combination of $Ru(bpy)_3^{2+}$ photosensitizer (bpy = 2,2'-bipyridine) and $S_2O_8^{2-}$ primary electron acceptor.[9,10]

Among the most employed ligands to stabilise the iridium centres along the oxygenic catalytic routine there are N-heterocyclic carbenes (NHCs), in virtue of their expected robustness and their sigma carbon-to-metal (C→M) donating character, combined with a π metal-to-carbon (M→C) retrodonation.[11] These features allow the stabilization of both low and high oxidation states of the metal centre.[12] Iridium(III) complexes with carbene ligands have been indeed proposed in combination with chemical oxidants.[3,4,13] With the aim of providing a bidentate chelating scaffold for the iridium centre potentially useful towards water oxidation catalysis,[13,14] we previously investigated the iridium complex **1a**, bearing the N-heterocyclic dicarbene ligand 1,1'-dimethyl-3,3'-ethylenediimidazol-2,2'-diylidene (Scheme 1). Our previous investigation evidenced a higher reactivity for **1a** in the presence of chemical oxidants with respect to the analogous iridium species where the diNHC ligand has a methylene linker between the imidazole rings;[14] in addition, **1a** was the first iridium coordination complex to be employed in light driven water oxidation employing the $Ru(bpy)_3^{2+}$ / $S_2O_8^{2-}$ cycle.[14] A combination of kinetic analysis, UV-Vis and EPR spectroscopy, dynamic light scattering (DLS) experiments suggested the occurrence of a homogeneous pathway with **1a**, both employing dark chemical oxidants and in the photogenerated $Ru(bpy)_3^{2+}$ / $S_2O_8^{2-}$ systems.

In this work, we expand the scope of Ir(III) diNHC complexes in light-driven water oxidation catalysis by investigating the two novel species **2** and **3** (Scheme 1), where the diNHC ligands are 1,1'-dimethyl-3,3'-ethylene-5,5'-dibromodiimidazol-2,2'-diylidene and 1,1'-dimethyl-dibenzimidazol-2,2'-diylidene, respectively. The presented results include: (i) a photon management analysis[15] of light-driven water oxidation with **1a**, allowing the optimisation of the

[a] Department of Chemical Sciences, University of Padova, via Marzolo 1, 35131 Padova, Italy.andrea.sartorel@unipd.it; cristina.tubaro@unipd.it
[b] Department of Chemical and Pharmaceutical Sciences, University of Ferrara, and Centro Interuniversitario per la Conversione Chimica dell'Energia Solare (SOLARCHEM), sez. Di Ferrara, via L. Borsari 46, 44121 Ferrara, Italy. mirco.natali@unife.it
[c] Department of Chemistry, Life Sciences and Environmental Sustainability, University of Parma, Parco Area delle Scienze 17/A, 43124 Parma, Italy.

† Electronic Supplementary Information (ESI) available: X-ray data and characterisation of **1**-**3**, details of photoinduced oxygen evolution experiments. See DOI: 10.1039/x0xx00000x

overall quantum yield (we have recently reported a quantum efficiency up to 64% with the **Ir-blue** dinuclear catalyst based on the 2-(2'-pyridyl)-2-propanoate (pyalc) ligand);[15] (ii) a reactivity trend in the **1**-**3** series that follows the electron donating character of the diNHC ligand (as proven by ^{13}C NMR carbene carbon chemical shift[16,17] and reduction potentials of the iridium complexes), with an order **1a** > **2** > **3** both in terms of initial rate of oxygen production and total amount of oxygen production, both at low and high photon flux; (iii) a consistent trend in the electron transfer rate from iridium species to photogenerated $Ru(bpy)_3^{3+}$, as proven by laser flash photolysis; (iv) the evolution of **1a** into the mononuclear iridium species involving progressive modification of both Cp* and diNHC ligand, as proven by combining UV-Vis, mass spectrometry and ^1H-NMR analysis.

Results and discussion

Synthesis of the iridium(III) complexes

The synthesis of complexes **1a** and **1b** (**1b** is the dicationic complex analogue of **1a**, with the chloride ligand substituted by an acetonitrile molecule) was previously reported.[14] Following a similar synthetic protocol, the novel iridium(III) complexes **2** and **3** were isolated in 70-83% yield by transmetalation of the di(N-heterocyclic carbene) ligand (diNHC) from the corresponding dinuclear silver(I) complexes (Scheme 1). The last ones were synthesised adapting standard procedures,[18] i.e. reaction of the bis(azolium) precursors with Ag_2O; the detailed experimental conditions for the synthesis of the silver complexes and their characterisation are reported in the Supplementary material. The transmetalation reaction affords iridium(III) mononuclear cationic complexes with the dicarbene ligand chelating the metal centre.

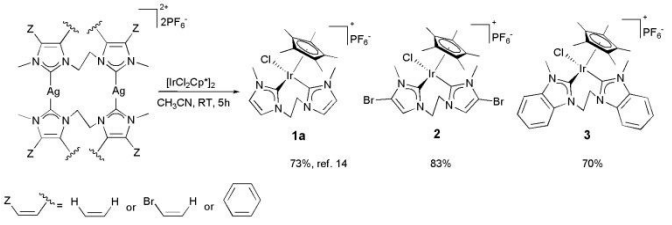

Scheme 1. Ir(III) complexes **1**-**3** with chelating diNHC ligands synthesised and employed in this work.

The crystal structures of the novel iridium(III) complexes, **2** and **3**, have been fully elucidated by X-ray diffraction analysis. The ORTEP views of the complexes are reported in Figures 1 and 2 together with the atomic labelling scheme. Considering the centroid of the Cp* ring (CT), the iridium atom shows a distorted tetrahedral environment. The three bond angles at the iridium atom involving the centroid of the Cp* ring (CT–Ir–$C_{carbene}$ and CT–Ir–Cl) are wider than the other three ($C_{carbene}$–Ir–$C_{carbene}$ and $C_{carbene}$–Ir–Cl), probably as a consequence of the steric hindrance exerted by the Cp* ring. The complex assumes a three-legged piano-stool structure with the dicarbene ligand engaged in two positions and the chloride in the remaining one. The bond lengths and angles are all in agreement with those reported for similar Ir–NHC complexes.[19,20] The monocationic nature of the obtained Ir(III) complexes has been confirmed also by means of matrix assisted laser desorption ionisation mass spectrometry (MALDI-MS, under positive mode), in which the main signal at *m/z* = 707/713 and 651/655 are attributed to the ions $[IrCp^*Cl(diNHC)]^+$ of **2** and **3**, respectively, as demonstrated by the calculated isotopic patterns (see ESI). In the ^1H NMR spectra the hydrogens of the ethylene bridge give an AA'XX' system, thus indicating a rigid arrangement of the chelating dicarbene ligand, with a slow interconversion of the 7-member metallacycle. In the ^{13}C NMR spectra the coordinated carbene carbon is located at 149.4 and 160.7 ppm for **2** and **3** respectively, in the typical range of carbene carbons coordinated to Ir(III) centres. The resonance of the benzimidazol-2-ylidene carbene carbon in **3** is shifted more than 10 ppm downfield compared to the equivalent signal in the analogous imidazol-2-ylidene complex **1a** (146.8 ppm); this could be ascribed to the reduced electron density on the N-heterocyclic ring caused by the condensed aryl group. Furthermore, it has been demonstrated that the carbene carbon chemical shift in the ^{13}C NMR spectra can be used to evaluate the donor ability of the ligand;[16,17] in particular the electron donating character of the three diNHC ligands here reported follows the order imidazol-2-ylidene > 5-bromo-imidazol-2-ylidene > benzimidazol-2-ylidene. Cyclic voltammetry (CV) of the iridium(III) complexes further support the observed trend in the electron density on the metal centre. CVs in acetonitrile show a reversible oxidation attributed to the Ir(IV)/Ir(III) couple at $E_{1/2}$ 1.40, 1.50 and 1.53 V (vs. Ag/AgCl) for **1a**, **2** and **3** respectively (these values are shifted to lower potentials in the presence of aqueous medium, vide infra). The electron density on the metal centre decreases in the order **1a** > **2** > **3**, thus consistently with the electron donor ability of the diNHC ligand found with the NMR measurements.

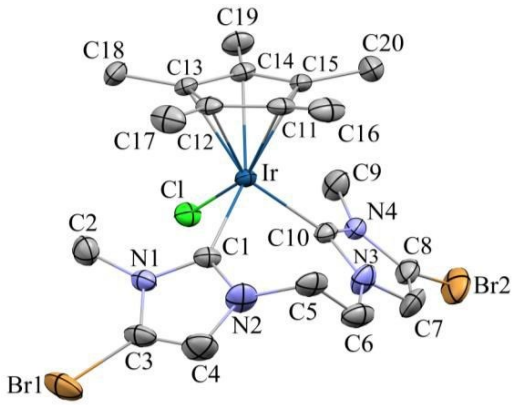

Figure 1. ORTEP view of the cationic complex **2**, ellipsoids are drawn at their 30 % probability. Hydrogen atoms and PF_6^- anions have been omitted for clarity. Most significant distances (Å) and angles (°): Ir-Cl 2.429(1); Ir-$C_{carbene}$ 2.066(5) and 2.044(5); Ir-CT 1.940. C1-Ir-C10 91.5(2); CT-Ir-Cl 121.46; $C_{carbene}$-Ir-Cl 88.6(1) and 87.2(1); CT-Ir-$C_{carbene}$ 128.37 and 127.39; γ 57.09. CT=centroid of the pentamethycyclopentadienyl ligand. γ=dihedral angle between the mean planes of the NHC moieties.

View Article Online
DOI: 10.1039/C9DT04841C

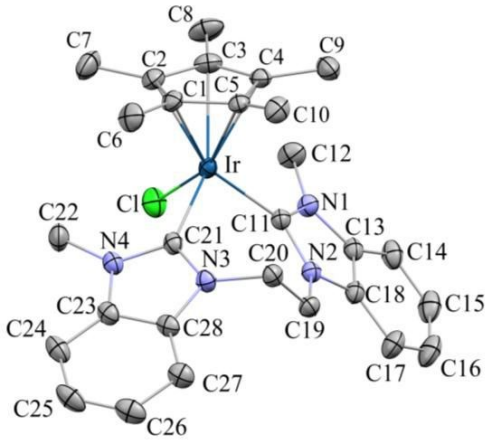

Figure 2. ORTEP view of the cationic complex 3, ellipsoids are drawn at their 30 % probability. Hydrogen atoms and PF_6^- anions have been omitted for clarity. Most significant distances (Å) and angles (°): Ir-Cl 2.421(1); Ir-$C_{carbene}$ 2.021(3) and 2.059(4); Ir-CT 1.948. $C_{carbene}$-Ir-$C_{carbene}$ 92.8(1); CT-Ir-Cl 123.90; $C_{carbene}$-Ir-Cl 89.5(1) and 84.3(9); CT-Ir-$C_{carbene}$ 129.36 and 124.81; γ 53.45. CT=centroid of the pentamethycyclopentadienyl ligand. γ=dihedral angle between the mean planes of the NHC moieties.

Light driven water oxidation with 1a managing photon flux

The forerunner **1a** of the diNHC iridium complexes employed in this work, was the first iridium coordination compound to be considered in light assisted catalysis with the $Ru(bpy)_3^{2+}/S_2O_8^{2-}$ system.[14] Here, the photogenerated oxidant $Ru(bpy)_3^{3+}$, $E_{1/2}(Ru^{III}/Ru^{II})$ = 1.26 V vs NHE, is generated by oxidative quenching of $*Ru(bpy)_3^{2+}$ triplet excited state by the $S_2O_8^{2-}$ anion (see Scheme S1 in ESI for an extensive description of the system).[21–24] As recently pointed out,[9,15,25] the photon management in the $Ru(bpy)_3^{2+}/S_2O_8^{2-}$ cycle is pivotal to maximize the efficiency of the overall system, where the most indicative parameter is the quantum yield $\phi(O_2)$. Oxygen evolution experiments were thus performed under fixed conditions exploiting **1a** as the catalyst ([**1a**] = 50 μM, $[Ru(bpy)_3^{2+}]$ = 1 mM, $[S_2O_8^{2-}]$ = 5 mM, in 15 mL of 50 mM $Na_2SiF_6/NaHCO_3$ buffer, pH 5.2)[14,15] and solely changing the light intensity (blue LED with emission at 450 nm, full width at half-maximum 10 nm, 4.42×10^{-9} to 2.12×10^{-7} einstein s^{-1}).[15] As expected, markedly different oxygen evolution kinetics were observed, as shown in Figure 3 (see also Table 1).□

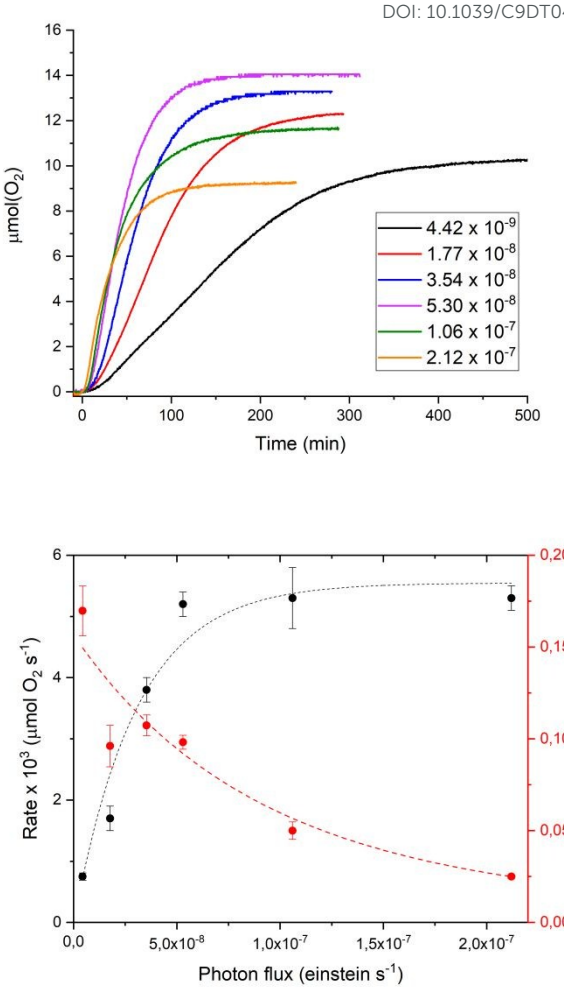

Figure 3. Oxygen evolution kinetics at different light intensity (4.42×10^{-9} to 2.12×10^{-7} einstein s^{-1}, with monochromatic LEDs emitting at 450 nm, FWHM = 10 nm). Conditions: 15 mL of 50 mM $Na_2SiF_6/NaHCO_3$ buffer, pH 5.2; $[Ru(bpy)_3^{2+}]$ = 1 mM; $[Na_2S_2O_8]$ = 5 mM; [**1a**] = 50 μM (introduced from a freshly prepared 2.5 mM solution in CH_3CN. The presence of an initial induction period before reaching the maximum rate of O_2 evolution is ascribed to the accumulation of photogenerated active intermediates to reach a steady state regime (in particular under low light intensity conditions), and to slow diffusion of O_2 to the headspace of the reactor.[14,15] In the graph, the irradiation is started at time = 0; in order to better appreciate the effect of light on the O_2 production, the O_2 level is also shown during the 10 minutes before starting irradiation (negative time, where the amount of O_2 stands below 0.05 μmol). Bottom: plot of the maximum rate of O_2 evolution (black dots) and of quantum yield (ϕ, red dots) vs photon flux.

View Article Online
DOI: 10.1039/C9DT04844C

Table 1. Parameters for the light-driven water oxidation reaction with the $Ru(bpy)_3^{2+}/S_2O_8^{2-}$ system in the presence of **1a**. Reaction conditions: 15 mL of 50 mM $Na_2SiF_6/NaHCO_3$ buffer, pH 5.2; $[Ru(bpy)_3^{2+}]$ = 1 mM; $[Na_2S_2O_8]$ = 5 mM; [**1a**] = 50 μM (loaded from a 2.5 mM solution in CH_3CN). Irradiation was performed with a series of six monochromatic LEDs emitting at 450 nm, modulating the intensity ($4.42\times10^{-9} \div 2.12\times10^{-7}$ einstein s^{-1}).

#	Photon flux, einstein·s^{-1}	$R_{MAX}\times10^3$,[a] μmol·s^{-1} (TOF×10^3, s^{-1})	Quantum yield, $\phi(O_2)$[b]	μmol O_2[c] (TON)
1	4.42×10^{-9}	0.75±0.06 (1.0±0.08)	0.17±0.01	10.3±0.4 (13.7±0.5)
2	1.77×10^{-8}	1.70±0.2 (2.27±0.3)	0.10±0.01	12.3±0.8 (16.4±1.0)
3	3.54×10^{-8}	3.8±0.2 (5.1±0.3)	0.108±0.006	13.3±0.7 (17.7±0.9)
4	5.30×10^{-8}	5.2±0.2 (6.9±0.3)	0.097±0.004	14.0±0.5 (18.7±0.7)
5	1.06×10^{-7}	5.3±0.5 (7.1±0.7)	0.050±0.005	11.6±0.7 (15.5±0.9)
6	2.12×10^{-7}	5.3±0.2 (7.1±0.3)	0.025±0.001	9.2±0.4 (12.3±0.5)

[a] R_{MAX} is determined by a linear fitting of the experimental traces, from 10 to 20 minutes after turning light on (an initial lag time of few minutes before reaching RMAX is ascribed to accumulation of photogenerated intermediates and to slow diffusion of O2 to the headspace of the reactor).[15] [b]Quantum yield determined from the ratio between the oxygen evolution rate and the photon flux (considering the optical density of the solution, all the photons are absorbed). [c]μmol of O_2 when the oxygen evolution kinetics reach the plateau. Experiments have been repeated three times in order to confirm reproducibility and to estimate the errors in the initial rate and in the total amount of oxygen produced.

As it was recently observed for the **Ir-blue** catalyst,[15] the maximum rate of oxygen evolution, R_{MAX} (and the associated maximum turnover frequency calculated per Ir centre), the total amount of O_2 produced (and the associated turnover number calculated per Ir centre) and the quantum yield of the process (calculated from the ratio between the maximum oxygen evolution rate and the absorbed photon flux) all depend on light intensity, see Table 1.

In particular, focusing on the maximum rate of O_2 evolution, R_{MAX}, two limiting regimes are observed (Figure 3, bottom; R_{MAX} is determined by a linear fitting of the kinetic profiles between 10 to 20 minutes after light irradiation): one below a photon flux threshold of 5×10^{-8} einstein s^{-1}, where a linear trend of R_{MAX} vs photon flux is observed; the second one above photon flux of 5×10^{-8} einstein s^{-1}, where the R_{MAX} shows an almost constant value (in the range 5.2 – 5.3×10^{-3} μmol(O_2) s^{-1}) not dependent on the photon flux, where **1a** reaches the maximum turnover frequency (TOF) of 7.1±0.3 ×10^{-3} s^{-1}, a half value with respect to the one observed for the **Ir-blue** catalyst under the same conditions.[15] This overall trend is attributed to a change of limiting steps, with the first segment at low light intensity where light is a limiting reagent, while in the second segment a chemical rate determining step is likely associated to the saturation of the TOF values. Optimal exploitation of light occurs at low light intensity, where a quantum yield up to 0.17±0.01 is observed; according to the postulated mechanism of oxygen production, where two photons are required to generate four oxidizing equivalent to generate oxygen, this value corresponds to a quantum efficiency of 34±2%.[23] Under these conditions, the O_2 production lasts for ca 2 h (except under the conditions at the lowest photon flux, where the O_2 evolution lasts for ca 6 h) before reaching a plateau, mainly ascribed to competitive degradation pathways of $Ru(bpy)_3^{2+}$ photosensitizer, leading to loss of photochemical activity. Indeed, UV-Vis traces of the spent reaction mixtures confirm an abatement of the metal-to-ligand charge transfer band of $Ru(bpy)_3^{2+}$ (Figure S1).[26,27] As a consequence, under the conditions adopted, the O_2 yield based on persulfate conversion is found in the range 24.5 – 37.3%, and the total turnover number per iridium centre falls between 12.3 – 18.7 (in the $Ru(bpy)_3^{2+}/S_2O_8^{2-}$ cycle, the maximum TON achievable is given by $[S_2O_8^{2-}]\times0.5/[Ir]$, equal in the present case to a value of 50).[15]

Light driven water oxidation with 1-3

The activity of **2** and **3** was then evaluated and compared to **1a**, in order to verify possible electronic effects of the different diNHC ligands on light-driven water oxidation catalysis. In particular, considering the previous evidence on the importance of light management, the oxygen evolution experiments have been conducted under a high (1.06×10^{-7} einstein s^{-1}) and low (1.77×10^{-8} einstein s^{-1}) photon flux, adopting the conditions previously reported (15 mL of 50 mM $Na_2SiF_6/NaHCO_3$ buffer, pH 5.2; $[Ru(bpy)_3^{2+}]$ = 1 mM; $[Na_2S_2O_8]$ = 5 mM; [Ir] = 50 μM, irradiation with blue LED), see Table 2;[14,15] the oxygen evolution traces are reported in Figure 4.

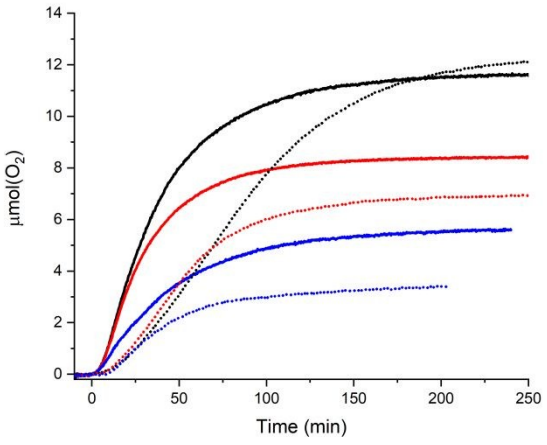

Figure 4. Oxygen evolution kinetics with **1a** (black), **2** (red) and **3** (blue) at different light intensity (dotted traces at 1.77×10^{-8} einstein s^{-1}, solid traces at 1.06×10^{-7} einstein s^{-1}, with monochromatic LEDs emitting at 450 nm, FWHM = 10 nm). Conditions: 15 mL of 50 mM $Na_2SiF_6/NaHCO_3$ buffer, pH 5.2; $[Ru(bpy)_3^{2+}]$ = 1 mM; $[Na_2S_2O_8]$ = 5 mM; [**Ir**] = 50 μM (introduced from a freshly prepared 2.5 mM solution in CH_3CN).

In particular, under both high and low illumination conditions, the reactivity trend in terms of R_{MAX} (and thus of TOF) and of the total amount of O_2 produced (and thus of TON) follows the electron donating character of the dicarbene ligands (evaluated by the aforementioned ^{13}C carbene carbon chemical shift and reduction potential of the Ir(IV)/(III) couple), with the reactivity order **1a** > **2** > **3**. The donating ability of the ligand scaffold is indeed recognised as an important feature in order to generate high valent species at low potentials.[28]

Table 2. Parameters for the photo-driven water oxidation reaction catalysed by **1a** - **3**.

Ir	Low light intensity, 1.77×10^{-8} einstein s^{-1}		High light intensity, 1.06×10^{-7} einstein s^{-1}		
	R_0×10^3,[a] µmols^{-1} (TOF×10^3(s^{-1}))	µmol O_2[a] (TON)	R_0×10^3,[a] µmols^{-1} (TOF×10^3(s^{-1}))	µmol O_2[a] (TON)	k_{ET} [b] /10^4, M^{-1}s^{-1}
1a	1.7±0.2 (2.3±0.3)	12.3±0.8 (16.4±1.0)	4.0±0.4 (5.3±0.5)	11.6±0.7 (15.5±0.9)	6.1±0.3
2	1.5±0.2 (2.0±0.3)	6.8±0.4 (9.1±0.5)	3.6±0.3 (4.8±0.4)	8.4±0.2 (11.2±0.3)	5.5±0.015
3	1.1±0.2 (1.5±0.3)	3.3±0.4 (4.4±0.5)	1.7±0.1 (2.3±0.1)	5.6±0.3 (7.5±0.4)	4.2±0.08

[a]Photochemical reaction conditions: 15 mL of 50 mM Na_2SiF_6/$NaHCO_3$ buffer, pH 5.2; [$Ru(bpy)_3^{2+}$] = 1 mM; [$Na_2S_2O_8$] = 5 mM; [Ir] = 50 µM (loaded from a 2.5 mM solution in CH_3CN). Irradiation was performed with a series of six monochromatic LEDs emitting at 450 nm, see ESI. Experiments have been repeated three times in order to confirm reproducibility and to estimate the errors in the initial rate and in the total amount of oxygen produced. [b]Bimolecular rate constants k_{ET} for the primary electron transfer from Ir(III) species to photogenerated $Ru(bpy)_3^{3+}$ (hole scavenging), determined by laser flash photolysis (excitation at 355 nm) of 25/75 acetonitrile/10 mM Na_2SiF_6/$NaHCO_3$ buffer (pH 5.2) mixtures containing 50 µM $Ru(bpy)_3Cl_2{\cdot}6H_2O$, 50 mM $Na_2S_2O_8$, and 1-2 mM iridium complex.

This reactivity trend was maintained also in the rate of electron transfer from the iridium species to photogenerated $Ru(bpy)_3^{3+}$, namely the first light-driven electron transfer step initiating catalysis.[23] The bimolecular rate constants for such an electron transfer process have been determined by laser flash photolysis following the time-evolution of the MLCT bleaching at 450 nm, characteristic of the formation of $Ru(bpy)_3^{3+}$ upon oxidative quenching of excited $Ru(bpy)_3^{2+}$ by $S_2O_8^{2-}$. A bleach recovery is indeed indicative of reaction of $Ru(bpy)_3^{3+}$ with the iridium species. Under pseudo first order conditions ([Ir(III)] >> [Ru(III)]), it is possible to fit the traces with monoexponential functions, leading to the determination of a pseudo-first order rate constant k_{obs}. The bimolecular rate constant for the electron transfer can be then extracted from the initial concentration of iridium species. In order to compare the kinetic response within the series of iridium complexes **1a-3** we chose a suitable solvent mixture providing substantial solubility to all compounds at concentrations where appreciable hole scavenging ability can be accurately determined. Laser flash photolysis experiments were thus performed upon excitation at 355 nm of 25/75 acetonitrile/10 mM Na_2SiF_6/$NaHCO_3$ buffer (pH 5.2) mixtures containing 50 µM $Ru(bpy)_3Cl_2{\cdot}6H_2O$, 50 mM $Na_2S_2O_8$ and the iridium complex. In Figure 5, top, the kinetic traces of the bleach recovery at 450 nm are reported for complex **1a** as an example, those of the other iridium complexes are reported in the ESI (Figure S2). In Figure 5, bottom, the plot of the pseudo-first order rates (k_{obs}) vs. the concentration of iridium complex is depicted, from which the bimolecular rate constant k_{ET} can be extracted. In particular, values of k_{1a} = (6.1±0.3)×10^4 M^{-1}s^{-1}, k_2 = (5.5±0.015)×10^4 M^{-1}s^{-1}, k_3 = (4.20±0.08)×10^4 M^{-1}s^{-1} can be estimated for the electron transfer to $Ru(bpy)_3^{3+}$ from **1a**, **2**, and **3**, respectively, showing a trend in perfect agreement with the one expected on the basis of the electronic effect of the diNHC ligands.§

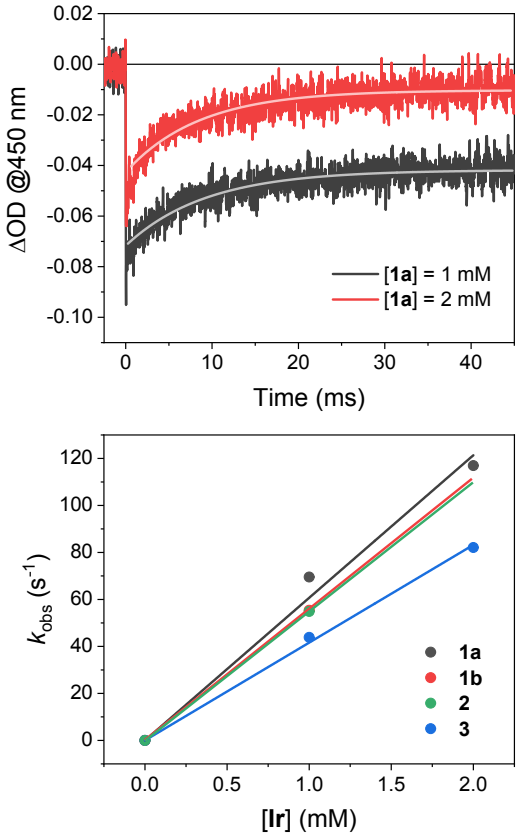

Figure 5. Kinetic traces at 450 nm obtained by laser flash photolysis (excitation at 355 nm) of 25/75 acetonitrile/10 mM Na_2SiF_6/$NaHCO_3$ buffer (pH 5.2) mixtures containing 50 µM $Ru(bpy)_3^{2+}$, 50 mM $Na_2S_2O_8$, and 1-2 mM **1a** (top). Plot of the pseudo-first order rates vs. the concentration of the iridium complex for the estimation of the bimolecular rate constant (bottom).

View Article Online
DOI: 10.1039/C9DT04841C

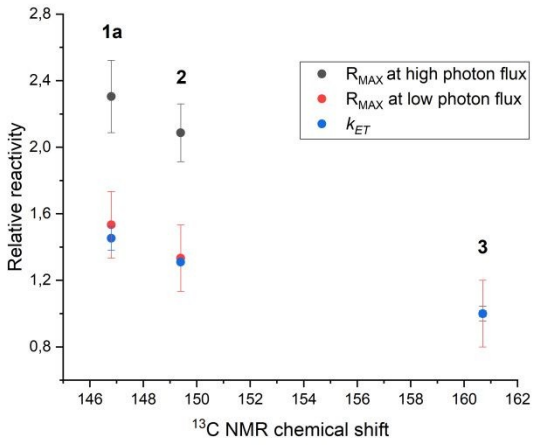

Figure 6. Relative reactivity of **1**-**3** in terms of R_{MAX} at high photon flux (black dots), R_{MAX} at low photon flux (red dots), and bimolecular k_{ET} versus the ^{13}C carbene chemical shift. The relative reactivity is given by the R_{MAX} and k_{ET} key performance indicators normalised with the ones observed for **3**.

The measured rate constants for electron transfer to $Ru(bpy)_3^{3+}$ deserve a further comment. These are more than 4 orders of magnitude lower with respect to those expected for diffusion-controlled processes and strongly point towards a reaction-controlled regime of the electron transfer from the Ir complex to $Ru(bpy)_3^{3+}$. The slow electron transfer kinetics can be likely ascribed to the low driving force of the process (see the CV traces in the presence of the aqueous buffer in Figure S3 in ESI), confirmed also by the incomplete recovery of the Ru(III) bleaching at 450 nm particularly at the lower iridium concentrations,[29] combined with a significant reorganization energy associated to the oxidation step of the iridium species. Furthermore, under the present kinetic regime, the positive charge of the Ir complexes may also hamper the formation of the activated complex for electron transfer with $Ru(bpy)_3^{3+}$ thus additionally contributing to the apparent kinetic inertness. The comparable rate constants measured for **1a** and **1b** ($k_{\mathbf{1b}}$ = $(5.6\pm0.2)\times10^4$ $M^{-1}s^{-1}$) clearly rules out a contribution of the nature of the apical ligand on the reorganization energy.§§ On the other hand, this can be possibly attributed to the enhanced delocalization of the HOMO over the diNHC ligand and thus to the large molecular rearrangement accompanying electron transfer, as typically observed, e.g., in chelating iridium complexes.[30,31] Interestingly, these observations might also suggest that, beside thermodynamic reasons, the faster electron transfer kinetics observed for the [IrCp*(OH)(pyalc)] derivative,[15] where the pyalc bidentate ligand does not display Ir-C bonds, is also the result of the smaller reorganization energy associated to the iridium oxidation process.

We finally investigated the possibility to associate the reactivity of **1**-**3**, in terms of R_{MAX} at high and low photon flux, and of the k_{ET} to $Ru(bpy)_3^{3+}$, to an indicator of the electron donating effect of carbene. In particular, Figure 6 reports the normalised reactivity trend of **1a**-**3** versus the carbene ^{13}C chemical shift, where the values of R_{MAX} and k_{ET} key performance indicators have been normalised with respect to the ones observed for **3**, in order to allow their direct visualisation in a single graph. Despite the number of investigated Ir species does not allow to validate a correlation, the observed trend supports the importance of the donating effect of the carbene ligand, possibly leading to reactivity prediction and catalyst design and engineering.

Evolution of Ir species along the light activated cycle

The impact of the electronic character of the ligand in the photocatalytic reactivity of iridium complexes speaks in favour of a persistent presence of the initial diNHC ligand or of a derived moiety in the species that operate in the oxygenic cycle. This supports the previous converging evidence on light-driven oxygen evolution by **1a** pointing toward a molecular mechanism, involving an Ir(IV) intermediate characterised by electron paramagnetic resonance (EPR) spectroscopy.[14]

We further analysed the transformation of **1a** under irradiation conditions by UV-Vis spectroscopy. Irradiation with white light of a solution containing 0.2 mM **1a**, 1 mM $Ru(bpy)_3^{2+}$ and 5 mM $S_2O_8^{2-}$, in 50 mM Na_2SiF_6/$NaHCO_3$ buffer at pH 5.2 containing 10 % acetonitrile, leads to the spectral changes reported in Figure 7 (spectra are reported as differential traces, full spectra are reported in Figure S4 in ESI). These experiments provide the following pieces of information: (i) the modest bleaching centred at 450 nm is indicative of the regeneration of Ru(II) from Ru(III), upon oxidation of the iridium species; conversely, a prompt bleaching of the absorbance at 450 nm is observed in the absence of iridium complex (Figure S5 in ESI), indicative of accumulation of Ru(III);[15] (ii) the absence of intense absorption around 600 nm rules out the formation of iridium oxide nanoparticles under these conditions, confirming previous evidences;[14]¥ (iii) weak absorptions are observed raising in the 500-700 nm range which are markedly different from those observed for the dinuclear **Ir-blue** catalyst,[15] while it is more likely associable to mononuclear high valent Ir-species;[32,33] (iv) the absence of isosbestic points as well as the different kinetics of the ΔAbs variation at different wavelengths (Figure 6, bottom) very likely indicate a transformation of **1a** into more than one species.

It is worth highlighting that the nature and nuclearity of iridium species formed from iridium precursors along water oxidation conditions is strictly dependent on the organic ligand of the iridium centre. The formation of iridium dinuclear species under catalytic conditions has been observed when using the strongly electron donating pyalc ligand,[6,15] while multimetallic reactive species have been postulated by Macchioni and Albrecht for iridium species stabilised by pyridine/alkyl-substituted carbene ligands, when the alkyl substituent at the nitrogen atom is sufficiently long (> ethyl).[3,4] In these cases, prolonged lag time and complex kinetic regimes in O_2 production were typically observed.[4b,c] Conversely, high valent mononuclear species were postulated by Mukhopadhyay et al. in the case of a bidentate phenyl/imine based ligand.[33] In the present case, the UV-Vis characterisation above and the previously observed well-behaved first order kinetics of O_2 evolution[14] suggest the involvement of mononuclear species.

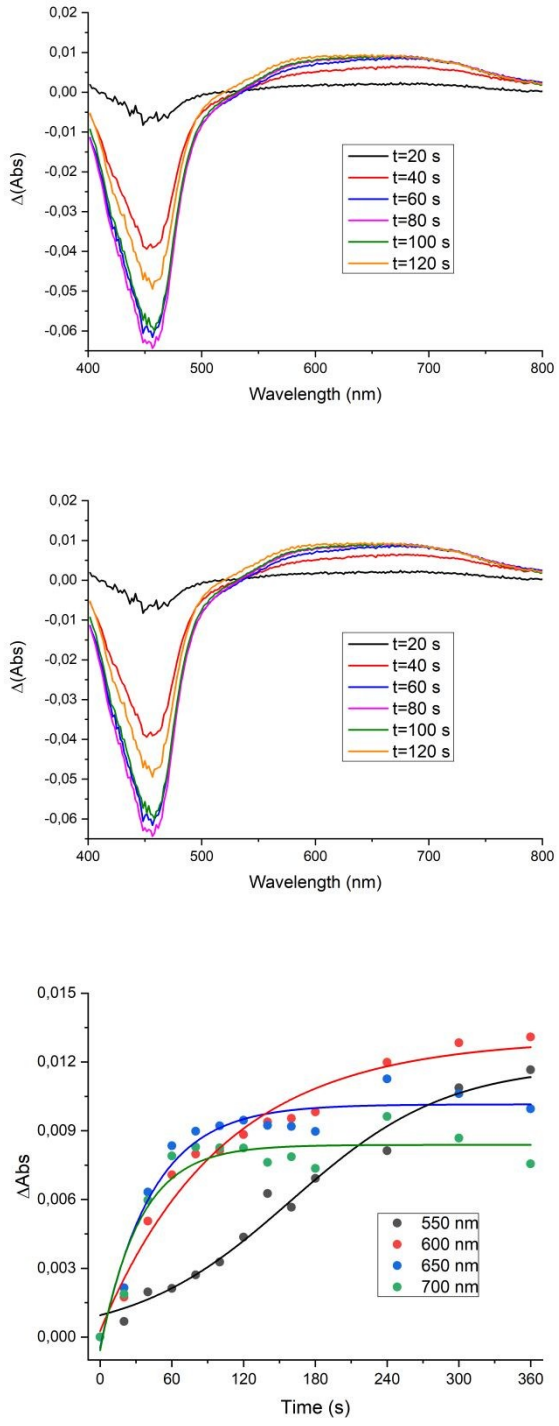

Figure 7. Differential absorbance spectra of a solution containing 200 μM **1a**, 1 mM $Ru(bpy)_3^{2+}$, 5 mM $S_2O_8^{2-}$, in 50 mM $Na_2SiF_6/NaHCO_3$ buffer at different times upon illumination with white light (3.8 mW cm^{-2} at 20 cm distance), at 20-120 s (top panel) and 120-360 s irradiation (middle panel). Bottom: plot of the ΔAbs at specific wavelengths vs time. The experiment was performed in a cuvette with 2 mm optical path.

The formation of mononuclear iridium species from **1a** along the irradiation within the $Ru(bpy)_3^{2+}$ / $S_2O_8^{2-}$ cycle was further confirmed by MALDI-MS.⊥ In particular, Figure 8 reports the spectra from a solution of 5 mM **1a**, 1 mM $Ru(bpy)_3^{2+}$ and 40 mM $S_2O_8^{2-}$, in 50:50 acetonitrile: 5 mM aqueous $Na_2SiF_6/NaHCO_3$ buffer at pH 5.2, before (black trace) and after (blue trace) irradiation with white light (the MALDI spectrum of $Ru(bpy)_3Cl_2$ is also reported in the red trace). The initial spectrum of the solution before irradiation (top panel, black spectrum in Figure 8) shows the main signals originated from **1a** at *m/z* = 551/553, attributed to the $[IrClCp^*diNHC]^+$ ion (hereafter $[M]^+$), and an envelope of signals at *m/z* between 513 and 519, which can be associated to the overlapping of the patterns of $[M\text{-}Cl]^+$ (loss of Cl·from M), $[M\text{-}HCl]^+$ (loss of HCl from M) and $[M\text{-}H_2Cl]^+$ (loss of HCl and H·from M) ions. Along irradiation, the parent signal at *m/z* = 551/553 progressively disappears, while new signals arise. In particular, a well-defined patter is observed at *m/z* = 461/463, blue spectra in Figure 7, registered at 15, 30 and 60 minutes of irradiation). This signal is observed to accumulate when treating **1a** with 100 equivalents $NaIO_4$ as a chemical oxidant, in aqueous solution (Figure S6 in ESI). Importantly, the isotopic pattern of this signal is consistent with mononuclear iridium species. Although an attribution could be speculative, the loss of a 90 mass from the parent species could be associated to the loss of a Cl· and of a neutral butene (C_4H_6) fragment.

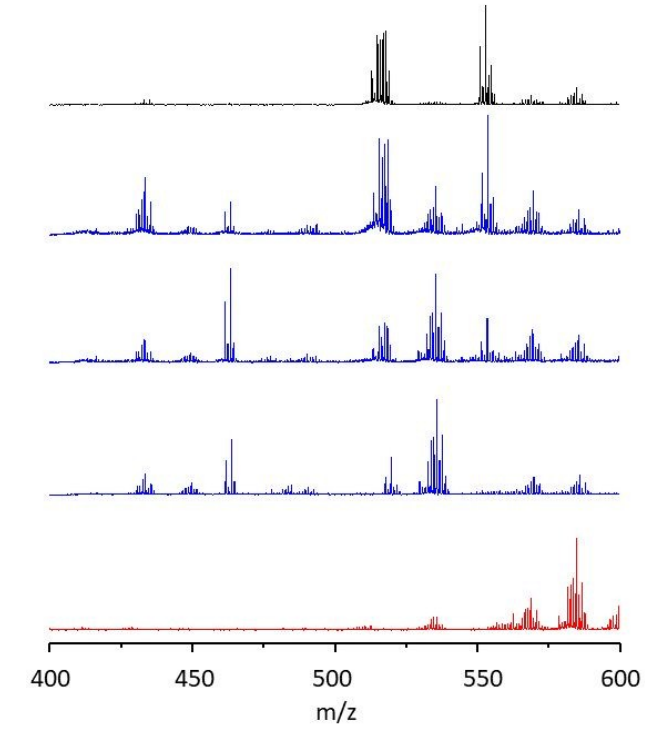

Figure 8. MALDI spectra of a solution containing 5 mM **1a**, 1 mM $Ru(bpy)_3^{2+}$ and 40 mM $S_2O_8^{2-}$, in 50:50 CH_3CN : 5 mM aqueous $Na_2SiF_6/NaHCO_3$ buffer at pH 5.2 before irradiation (black trace) and along irradiation with white light (blue traces, at 15, 30 and 60 minutes); the red trace reports the spectrum of $Ru(bpy)_3^{2+}$ under irradiation in the presence of $S_2O_8^{2-}$.

Indeed, the formation of mononuclear iridium species with a lower mass with respect to parent **1a** is likely associated to oxidative fragmentation of the organic ligands scaffold. In particular, the Cp* residue in the iridium complex is known to

decompose to CO_2 or to carboxylic acids in the harsh oxidizing conditions employing chemical oxidants.[34–36] More recently, acetic acid was identified as a degradation product of Cp* from Ir(pyalc) precursor under photochemical conditions with the $Ru(bpy)_3^{2+}/S_2O_8^{2-}$ cycle.[15] Indeed, acetic acid was observed to form along irradiation of the **1a**/$Ru(bpy)_3^{2+}/S_2O_8^{2-}$ system, from the growing of the singlet signal at 1.96 ppm in the ^{1}H-NMR spectrum (Figure S7 in ESI). Besides the formation of acetic acid, raising of signals around 1.5 ppm and at around 3 ppm was also observed. The former was previously attributed to oxidized derivatives of Cp*,[34] while the second one can be reasonably associated to methylene groups in a carbon bound to oxygen, still deriving from oxidation of the Cp*.[34]

Consistently, a progressive abatement of the Cp* signal at 1.7 ppm was observed. Importantly, a partial abatement of intensity was observed also for the signals of the diNHC ligand, and in particular of the (N)-CH_3 and (N)-CH_2- moieties; the signals of the C-H groups in the backbone of the heterocyclic ring show instead a slower change, consistent with the expected lower reactivity of these C-H groups toward hydrogen abstraction (Figure S8 in ESI).[37] In addition, the (N)-CH_2- CH_2-(N) scaffold could be subject to Hoffman type elimination, although this is considered more problematic for the azolium salts, precursors of the carbene ligands, rather than for carbenes coordinated to metal centres.[38-39] Therefore, a further engineering of the diNHC ligand should also consider to avoid the presence of aliphatic C-H, in particular when carbon is bound to nitrogen.

Conclusions

We have reported light driven water oxidation catalysis within the $Ru(bpy)_3^{2+}/S_2O_8^{2-}$ cycle by using [IrClCp*diNHC]PF_6 complexes **1**-**3**, with **2** and **3** being novel and structurally characterised complexes, where the iridium centre bears different N-heterocyclic dicarbene (diNHC) and a common pentamethylcyclopentadienyl (Cp*) ligands. As recently recognised,[9,15,25] the photon management is an important variable in order to optimise the quantum yield of the system, that reaches a notable value of 0.17±0.1 for **1a** under low irradiation intensity. Interestingly, the nature of the diNHC ligands impacts on the catalytic properties of the iridium complexes, with a reactivity trend that follows the donating character of the carbene. Indeed, both the rate of oxygen evolution (at both low and high photon flux) and the bimolecular rate constants of electron transfer to $Ru(bpy)_3^{3+}$ follow a trend **1a** > **2** > **3**, correlating with the carbene carbon chemical shift of the complexes, as an indicator of the donating character of the ligand. UV-Vis, MALDI-MS and ^{1}H-NMR characterisations indicate the evolution of **1a** to mononuclear iridium species with lower molecular weight, from the loss of fragments from the organic ligands. Strategies to further enhance the stability of the diNHC ligand should be thus considered, including the absence of aliphatic C-H groups bound to the nitrogen atoms.

Conflicts of interest

View Article Online
DOI: 10.1039/C9DT04841C

There are no conflicts to declare.

Experimental

The reagents were purchased from Sigma-Aldrich as high-purity products and generally used as received, except for $[Ru(bpy)_3]Cl_2$ that was re-crystallised twice from acetonitrile; all solvents were used as received as technical grade solvents. The precursor $[IrCl_2Cp^*]_2$, the bis(benzimidazolium) precursor and the iridium(III) complex **1a** and **1b** were prepared according to literature procedures. The NMR spectra were recorded on a Bruker Avance 300 (300.1 MHz for ^{1}H, 75.5 MHz for ^{13}C and 121.5 MHz for ^{31}P) at 298 K unless otherwise stated; chemical shifts (δ) are reported in units of ppm relative to the residual solvent signals (for ^{1}H and ^{13}C). ESI-MS analyses were performed using a LCQ-Duo (Thermo-Finnigan) operating in positive ion mode. MALDI-Ms were performed with a 4800 MALDI TOF/TOF Analyzer from AB Sciex. Elemental analysis were carried out by the microanalytical laboratory of Chemical Sciences Department (University of Padova) with a ThermoScientific FLASH 2000 apparatus. Cyclic voltammetry experiments were performed by using a BASi EC-epsilon potentiostat. A standard three-electrode electrochemical cell was used. Potentials were referenced to an Ag/AgCl/3M NaCl, reference electrode. A glassy carbon electrode (3 mm diameter, geometric surface area: 7 mm^2) and a Pt wire were used, respectively, as working and auxiliary electrode.

Dynamic light Scattering (DLS) experiments were performed with a Malvern Zetasizer Nano-S instrument, equipped with a quartz cuvette thermostated at 25°C; laser wavelength 633 nm. Nanosecond transient absorption measurements were performed with a custom laser spectrometer comprised of a Continuum Surelite II Nd:YAG laser (FWHM 6 –8 ns) with a frequency doubled (532 nm) or triple (355 nm) options, an Applied Photo-physics xenon light source including a mod. 720 150 W lamp housing, a mod. 620 power-controlled lamp supply and a mod. 03-102 arc lamp pulser. Laser excitation was provided at 90° with respect to the white light probe beam. Light transmitted by the sample was focused onto the entrance slit of a 300 mm focal length Acton SpectraPro 2300i triple grating, flat field, double exit monochromator equipped with a photomultiplier detector (Hamamatsu R3896) and a Princeton Instruments PIMAX II gated intensified CCD camera, using an RB Gen II intensifier, an ST133 controller and a PTG pulser. Signals from the photomultiplier (Hamamatsu R928) were processed by means of a Teledyne LeCroy 604Zi digital oscilloscope (400 MHz, 20 GS/s).

Water oxidation experiments were performed in a home-made cylindrical glass reactor, employing 15 mL of 50 mM $NaHCO_3/Na_2SiF_6$ aqueous buffer (pH 5.2) containing $[Ru(bpy)_3]Cl_2$ (1 mM), $Na_2S_2O_8$ (5 mM) and the iridium species. The solution was deoxygenated with nitrogen for about 20 minutes and allowed to equilibrate at 25 °C under the exclusion of light, and then irradiated with a series of six monochromatic LEDs emitting at 450 nm and with FWHM = 10 nm (LED450–06

from Roithner Lasertechnik GmbH; photon flux was modulated in the range 4.42×10^{-9} to 2.12×10^{-7} einstein·s^{-1}; the irradiation power of the LEDs was measured with an AvaSpec-2048 Fiber Optic Spectrometer from Avantes). Oxygen evolution was monitored with a FOXY-R-AF probe inserted into the reaction headspace and interfaced with Neofox Real-Time software for data collection.

Synthesis of 2 and 3

A solution of $[IrCl_2Cp^*]_2$ (0.1 mmol) in acetonitrile (15 mL) was added to a solution of the proper silver(I) complex (0.1 mmol) in acetonitrile (15 mL); the resulting suspension was stirred at room temperature under the exclusion of light for 5 h. The mixture was then filtered through Celite and the filtrate concentrated under reduced pressure. Addition of diethyl ether (10 mL) afforded the product, which was filtered off and dried in vacuum.

2. Yellow solid. Yield 83%. ^{1}H NMR (CD_3CN, 25 °C, ppm): δ = 1.62 (s, 15H, Cp*-C*H*$_3$), 3.80 (s, 6H, NC*H*$_3$), 4.30 – 4.59 (AA'XX' system, 4H, C*H*$_2$), 7.29 (s, 2H, C*H*). ^{13}C{^{1}H} NMR (CD_3CN, 25 °C, ppm): δ = 8.0 (Cp*-*C*H$_3$), 37.5 (N*C*H$_3$), 48.9 (*C*H$_2$), 94.5 (Cp*-*C*), 108.1 (*C*H), 123.5 (*C*), 149.4 (N*C*N). ESI-MS (positive ions) *m*/*z*: 711 [Cp*IrCl(diNHC)]$^+$. Anal. Calcd for $C_{20}H_{27}Br_2ClF_6IrN_4P$: C, 28.10; H, 3.19; N, 6.56%. Found: C, 28.52; H, 3.46; N, 6.57%.

3. Yellow solid. Yield 70%. ^{1}H NMR (CD_3CN, 25 °C, ppm): δ = 1.72 (s, 15H, Cp*-C*H*$_3$), 4.05 (s, 6H, NC*H*$_3$), 4.86 – 4.96 (AA'XX' system, 4H, C*H*$_2$), 7.42 (m, 4H, Ar-C*H*), 7.59 (m, 4H, Ar-C*H*). ^{13}C{^{1}H} NMR (CD_3CN, 25 °C, ppm): δ = 14.8 (Cp*-*C*H$_3$), 36.3 (N*C*H$_3$), 45.7 (*C*H$_2$), 95.3 (Cp*-*C*), 111.3 (*C*H), 111.8 (*C*H), 124.7 (*C*H), 124.9 (*C*H), 135.4 (*C*), 136.5 (*C*), 160.7 (N*C*N). ESI-MS (positive ions) *m*/*z*: 653 [Cp*IrCl(diNHC)]$^+$. Anal. Calcd for $C_{28}H_{33}ClF_6IrN_4P$: C, 42.10; H, 4.17; N, 7.02%. Found: C, 46.01; H, 3.66; N, 6.57%.

X-ray crystal structure determination of 2 and 3.

The crystallographic data for all complexes were collected on a Bruker Smart Apex II single-crystal diffractometer working with monochromatic Mo-Kα radiation and equipped with an area detector. The structures were solved by direct methods and refined against F^2 with SHELXL-2014/7 with anisotropic thermal parameters for all non-hydrogen atoms. Idealized geometries were assigned to the hydrogen atoms. Details for the X-ray data collection are reported in the supporting information. Crystallographic data have been deposited with the Cambridge Crystallographic Data Centre as supplementary publication: complex 2 (1972605) and complex (1972606). Copies of the data can be obtained free of charge on application to the CCDC, 12 Union Road, Cambridge CB2 1EZ, U.K. (fax, (+44) 1223 336033; e-mail, deposit@ccdc.cam.ac.uk).

Acknowledgements

We thank Prof. Gary W. Brudvig (Yale) for fruitful discussions. This work was supported by the Department of Chemical Sciences at the University of Padova (P-DISC "Phoetry" #10BIRD2018-UNIPD) and by Fondazione Cariparo ("Synergy", Progetti di Eccellenza 2018).

Notes and references

☐ The simultaneous presence of the Ir complex, Ru photosensitiser, $S_2O_8^{2-}$ and light is necessary to activate oxygen production. Concerning possible thermal effects, the blue emitting LED used as the light source do not lead to an appreciable warming of the solution, and the temperature of the solution stands in the range 20-25°C over the entire course of the experiment.

§ A slightly larger value for the bimolecular rate constant k_{1a} = $(2.9\pm0.01)\times10^5$ $M^{-1}s^{-1}$ was previously observed for compound **1a** under different experimental conditions, namely 10/90 acetonitrile/50 mM Na_2SiF_6/$NaHCO_3$ buffer (pH 5.2).[15] The observed difference very likely stems from the slight decrease in the driving force for the electron transfer process with a larger acetonitrile content.

§§ It has also to be noted that the nature of the apical ligand does not impact on the catalysis, since **1a** and **1b** do not show a significant change in the oxygen evolution catalysis.

¥ Major formation of colloidal species was ruled out also by dynamic light scattering analysis of the spent reaction mixtures, resulting in scattering intensity below the detection limit of the instrument, thus confirming previous evidence (see ref. 14). Absence of significant scattering was observed also for the solutions before irradiation.

⊥ MALDI was used to characterise the Ir-blue dinuclear species with pyalc ligand, and therefore appears a promising mass spectrometry technique to discriminate between mononuclear and polynuclear iridium species, see ref. 40

1 A. Macchioni, *Eur. J. Inorg. Chem.*, 2019, 7–17.
2 N. D. McDaniel, F. J. Coughlin, L. L. Tinker and S. Bernhard, *J. Am. Chem. Soc.*, 2008, **130**, 210–217.
3 J. A. Woods, R. Lalrempuia, A. Petronilho, N. D. McDaniel, H. Müller-Bunz, M. Albrecht and S. Bernhard, *Energy Environ. Sci.*, 2014, **7**, 2316–2328.
4 (a) R. Lalrempuia, N. D. McDaniel, H. Müller-Bunz, S. Bernhard and M. Albrecht, *Angew. Chemie - Int. Ed.*, 2010, **49**, 9765–9768. (b) I. Corbucci, A. Petronilho, H. Muller-Bunz, L. Rocchigiani, M. Albrecht and A. Macchioni, *ACS Catal.* 2015, **5**, 2714–2718. (c) I. Corbucci, F. Zaccaria, R. Heath, G. Gatto, C. Zuccaccia, M. Albrecht and A. Macchioni, *ChemCatChem* 2019, **11**, 5353-5361.
5 J. M. Thomsen, D. L. Huang, R. H. Crabtree and G. W. Brudvig, *Dalt. Trans.*, 2015, **44**, 12452–12472.
6 S. W. Sheehan, J. M. Thomsen, U. Hintermair, R. H. Crabtree, G. W. Brudvig and C. A. Schmuttenmaer, *Nat. Commun.*, 2015, **6**, article number: 6469.
7 G. Menendez Rodriguez, G. Gatto, C. Zuccaccia and A. Macchioni, *ChemSusChem*, 2017, **10**, 4503–4509.
8 H.-C. Chen, D. G. H. Hetterscheid, R. M. Williams, J. I. van der Vlugt, J. N. H. Reek and A. M. Brouwer, *Energy Environ. Sci.*, 2015, **8**, 975–982.
9 B. Limburg, E. Bouwman and S. Bonnet, *ACS Catal.*, 2016, **6**, 5273–5284.
10 I. Corbucci, K. Ellingwood, L. Fagiolari, C. Zuccaccia, F. Elisei, P. L. Gentili and A. Macchioni, *Catal. Today*, 2017, **290**, 10–18.
11 M. N. Hopkinson, C. Richter, M. Schedler and F. Glorius, *Nature*, 2014, **510**, 485–496.
12 X. Bugaut and F. Glorius, *Chem. Soc. Rev.*, 2012, **41**, 3511–3522.

13 A. R. Parent, T. P. Brewster, W. De Wolf, R. H. Crabtree and G. W. Brudvig, *Inorg. Chem.*, 2012, **51**, 6147–6152.
14 A. Volpe, A. Sartorel, C. Tubaro, L. Meneghini, M. Di Valentin, C. Graiff and M. Bonchio, *Eur. J. Inorg. Chem.*, 2014, 665–675.
15 A. Volpe, C. Tubaro, M. Natali, A. Sartorel, G. W. Brudvig and M. Bonchio, *Inorg. Chem.*, 2019, **58**, 16537–16545.
16 Q. Teng and H. V. Huynh, *Dalt. Trans.*, 2017, **46**, 614–627.
17 H. V. Huynh, Ed., *The Organometallic Chemistry of N-heterocyclic Carbenes*, Wiley, 2017.
18 C. Tubaro, A. Biffis, R. Gava, E. Scattolin, A. Volpe, M. Basato, M. M. Díaz-Requejo and P. J. Perez, *European J. Org. Chem.*, 2012, 1367–1372.
19 G. Su, X. K. Huo and G. X. Jin, *J. Organomet. Chem.*, 2011, **696**, 533–538.
20 M. Vogt, V. Pons and D. M. Heinekey, *Organometallics*, 2005, **24**, 1832–1836.
21 M. Natali, F. Nastasi, F. Puntoriero and A. Sartorel, *Eur. J. Inorg. Chem.*, 2019, 2027–2039.
22 I. Bazzan, A. Volpe, A. Dolbecq, M. Natali, A. Sartorel, P. Mialane and M. Bonchio, *Catal. Today*, 2017, **290**, 39–50.
23 A. Sartorel, M. Bonchio, S. Campagna and F. Scandola, *Chem. Soc. Rev.*, 2013, **42**, 2262–2280.
24 M. Natali, M. Orlandi, S. Berardi, S. Campagna, M. Bonchio, A. Sartorel and F. Scandola, *Inorg. Chem.* 2012, **51**, 7324–7331.
25 L. Francàs, R. Matheu, E. Pastor, A. Reynal, S. Berardi, X. Sala, A. Llobet and J. R. Durrant, *ACS Catal.*, 2017, **7**, 5142–5150.
26 C. T. Lin, W. Böttcher, M. Chou, C. Creutz and N. Sutin, *J. Am. Chem. Soc.*, 1976, **98**, 6536–6544.
27 P. K. Ghosh, B. S. Brunschwig, M. Chou, C. Creutz and N. Sutin, *J. Am. Chem. Soc.*, 1984, **106**, 4772–4783.
28 T. K. Michaelos, D. Y. Shopov, S. B. Sinha, L. S. Sharninghausen, K. J. Fisher, H. M. C. Lant, R. H. Crabtree and G. W. Brudvig, *Acc. Chem. Res.*, 2017, **50**, 952–959.
29 G. La Ganga, F. Puntoriero, S. Campagna, I. Bazzan, S. Berardi, M. Bonchio, A. Sartorel, M. Natali and F. Scandola, *Faraday Discuss.*, 2012, **155**, 177–190.
30 R. D. Costa, E. Ortí, H. J. Bolink, F. Monti, G. Accorsi and N. Armaroli, *Angew. Chemie - Int. Ed.*, 2012, **51**, 8178–8211.
31 I. González, M. Natali, A. R. Cabrera, B. Loeb, J. Maze and P. Dreyse, *New J. Chem.*, 2018, **42**, 6644–6654.
32 D. Y. Shopov, B. Rudshteyn, J. Campos, D. J. Vinyard, V. S. Batista, G. W. Brudvig and R. H. Crabtree, *Chem. Sci.*, 2017, **8**, 1642–1652.
33 S. Mukhopadhyay, R. S. Singh, A. Biswas and D. S. Pandey, *Chem. Commun.*, 2016, **52**, 3840–3843.
34 A. Savini, P. Belanzoni, G. Bellachioma, C. Zuccaccia, D. Zuccaccia and A. MacChioni, *Green Chem.*, 2011, **13**, 3360–3374.
35 C. Zuccaccia, G. Bellachioma, S. Bolaño, L. Rocchigiani, A. Savini and A. Macchioni, *Eur. J. Inorg. Chem.*, 2012, **2**, 1462–1468.
36 C. Zuccaccia, G. Bellachioma, O. Bortolini, A. Bucci, A. Savini and A. Macchioni, *Chem. - A Eur. J.*, 2014, **20**, 3446–3456.
37 S. J. Blanksby and G. B. Ellison, *Acc. Chem. Res.*, 2003, **36**, 255–263.
38 A. W. Salman, R. A. Haque, S. Budagumpi and H. Z. Zulikha, *Polyhedron* 2013, **49**, 200–206.
39 D. Tumelty, K. Cao and C. P. Holmes, *Org Lett* 2001, **3**, 83–86.
40 U. Hintermair, S. W. Sheehan, A. R. Parent, D. H. Ess, D. T. Richens, P. H. Vaccaro, G. W. Brudvig and R. H. Crabtree, *J. Am. Chem. Soc.* 2013, **135**, 10837–10851.

View Article Online
DOI: 10.1039/C9DT04841C

View Article Online
DOI: 10.1039/C9DT04841C

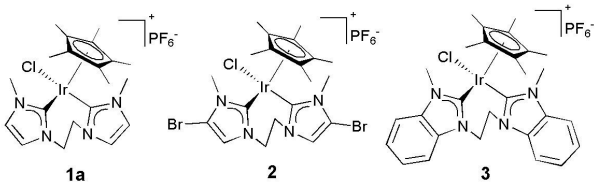

1a 2 3

Iridium complexes with N-heterocyclic dicarbene ligands have been investigated in light driven water oxidation catalysis within the $Ru(bpy)_3^{2+}/S_2O_8^{2-}$ cycle.